Chimica Techno Acta
published by Ural Federal University
eISSN 2411-1414; chimicatechnoacta.ru

ARTICLE
2021, vol. 8(2), № 20218204
DOI: 10.15826/chimtech.2021.8.2.04

ABO_4 type scheelite phases in $(Ca/Sr)MoO_4$ - $BiVO_4$ - $Bi_2Mo_3O_{12}$ systems: synthesis, structure and optical properties

Z.A. Mikhaylovskaya[a,b,*], E.S. Buyanova[b], S.A. Petrova[c], A.V. Klimova[a,b]

a: Zavaritsky Institute of Geology and Geochemistry of the Ural Branch of the Russian Academy of Sciences, 15 Ak. Vonsovskogo st., Ekaterinburg, 620016, Russia
b: Ural Federal University, 19 Mira st., Ekaterinburg, 620002, Russia
c: Institute for Metallurgy of the Ural Branch of the Russian Academy of Sciences, 101 Amundsena st., Ekaterinburg, 620016, Russia
* Corresponding author: zozoikina@mail.ru

This article belongs to the regular issue.

Abstract

The cation deficient complex oxides of $(Ca/Sr)MoO_4$ - $BiVO_4$ - $Bi_2Mo_3O_{12}$ triple system are promising photocatalysts and pigments. Compounds with general formula of $Ca_{1-1.5x-y}Bi_{x+y}\Phi_xMo_{1-y}V_yO_4$ and $Sr_{1-1.5x-y}Bi_{x+y}\Phi_xMo_{1-y}V_yO_4$ were synthesized by convention solid state technique in the range of 550-720 °C. Two wide regions of the solid solutions (ordinary and superstructured scheelite-type phases respectively) were found for each system. The diffuse scatering of homogeneous samples was investigated in the range of 190-1100 nm. Energy gaps calculated with linear approximation of Kubelka-Munk function decreases with bismuth and vanadium content.

Keywords

strontium bismuth molybdate
calcium bismuth molybdate
Kubelka-Munk method
energy gap

Received: 25.03.2021
Revised: 12.04.2021
Accepted: 28.04.2021
Available online: 29.04.2021

1. Introduction

Materials based on $CaMoO_4$ and $SrMoO_4$ are of interest for science and technology as catalysts and photocatalysts, scintillation detectors, solid-state lasers, pigments as well as for using in photoluminescent and microwave devices due to a wide variety of functional properties [1-8]. The latter strongly depend on not only the nature of dopants [2-3] but also on synthesis techniques employed [2,3,8] and a place of doping. The doping in different sublattice (Ca/Sr or Mo) and varying parameters of synthesis (temperatures, irradiation time, pH, speed of mixture, etc.) may cause distortion of MoO_4 polyhedra. This distortion, in turn, affects such physical and chemical properties as photocatalytic activity [8-10], optical and luminescence properties [2-3,11], conductivity [12], etc.

The most common way of substitution in ABO_4 complex oxides with scheelite structure is doping *A*-sublattice by trivalent Me^{3+} cations [3-4,6-7,13]. In this case, three basic charge compensation mechanisms are possible in ABO_4 scheelites: (1) formation of oxide ion interstitials ($A_{1-x}M_xBO_{4+x/2}$) [12]; (2) co-substitution on A or B sites by subvalent cations ($A_{1-2x}Me^{3+}{}_xMe^{+}{}_xO_4$ or $A_{1-x}Me^{3+}{}_xB_{1-x}Me^{5+}{}_xO_4$) [16-17,6]; (3) formation of cation vacancies ($A_{1-3x}M_{2x}\Phi_xBO_4$) [13-17]. Mechanism (3) was reported for rare earth molybdates $Ln_2Mo_3O_{12}$ ($Ln_{2/3}MoO_4$, x=1/3) with scheelite-type structure [14] and for a small number of completely investigated $A_{1-3x}M_{2x}\Phi_xMoO_4$ series where $0 < x \le 1/3$ [13,17]. But cation vacancies (Φ) and their ordering can influence not only structure, but also the physical and chemical properties of the molybdates, and, therefore, we pay close attention to them in the present work. The simultaneous use of mechanisms (2) and (3) have not been described yet. For this reason the present work is devoted to the synthesis and characterization Bi and V co-doped $CaMoO_4$ and $SrMoO_4$ obtained by mechanisms (2) and (3).

Previously, Sleight et al. [18] reported the $x = 0.04$ compositions of $(Ca/Sr)_{1-3x}Bi_{2x}\Phi_xMoO_4$ series with the tetragonal scheelite structure (sp. g. $I4_1/a$). Sleight assumed that solid solution limit could apparently go all the way to 0.333. The structure, microwave dielectric properties, conductivity and photocatalytic activity of $Ca_{1-3x}Bi_{2x}\Phi_xMoO_4$ series were investigated in [13,19]. Guo et al. [13] synthesized series of solid solutions $Ca_{1-3x}Bi_{2x}\Phi_xMoO_4$ ($0.005 \le x \le 0.20$), using a conventional ceramic method, and examined their microstructure and microwave dielectric properties. The $0 \le x \le 0.15$ compositions were found to be single-phase and to have scheelite structure with cationic vacancies [13,19] (the structural model of $Sr_{0.88}Bi_{0.08}MoO_4$ [18] was used). It was shown that Bi-doped samples exhibit improved values of the mi-

crowave quality factor (Qf). Vibrational spectroscopy results revealed large distortions of MoO_4 and BiO_8 polyhedra [13], with a strong correlation between substitutions in the cation (A^{n+}) sublattice and microwave dielectric properties of the $Ca_{1-3x}Bi_{2x}\Phi_xMoO_4$ series. Later, the powder X-ray and neutron diffraction patterns for compositions with $0.15 < x \leq 0.225$ were shown to exhibit a tetragonal supercell with $a_{sup} \approx \sqrt{5}a$, $c_{sup} \approx c$ where a and c are the tetragonal scheelite cell parameters [19]. This superstructural ordering results in the additional reflections on XRPD patterns detected by Guo et al. [13] and provided by ordering of Bi atoms and cationic vacancies [19]. Samples described with supercell showed maximal photocatalytic activity due to complex microstructure at grain surface and also showed a decrease of total conductivity as compared to samples with normal scheelite structure [19]. The conductive properties and structure of $Sr_{1-3x}Bi_{2x}\Phi_xMoO_4$ compositions ($0.025 \leq x \leq 0.225$) were described in [20]. The superstructural ordering was also observed for $0.15 \leq x \leq 0.4$. In Fourier-transformed infrared spectra of $Sr_{1-3x}Bi_{2x}\Phi_xMoO_4$, the general shifting of absorption bands caused by deformation of MoO_4 tetrahedra was observed. An increase of overall electrical conductivity with x was also observed. The activation energy decreased with x insignificantly (from ~1.2 to ~1.1eV), indicating that the charge carriers and conduction mechanism in $Sr_{1-3x}Bi_{2x}\Phi_xMoO_4$ generally were the same as in the parent compound $SrMoO_4$. Probably, the increase of conductivity was caused by the increase in the oxygen ion mobility provided by the distortion of MoO_4 polyhedra [20].

Synthesis of $Sr_{1-x}Bi_xMo_{1-x}V_xO_4$ results in the two-phase samples consisting of $BiVO_4$ (monoclinic) and $SrMoO_4$ phases [20]. In contrast, $Ca_{1-x}Bi_xMo_{1-x}V_xO_4$ single-phase solid solutions are observed for $0 \leq x \leq 0.9$ [6]. One possible reason of such discrepancy is that the dopants influence differently the composition and structure of strontium and calcium molybdates. The simultaneous presence of Bi and V in $Ca_{1-x}Bi_xMo_{1-x}V_xO_4$ oxide leads to the simultaneous expansion and contraction of its unit cell due to the replacement of calcium with bismuth and molybdenum with vanadium, respectively; as a result, the unit cell volume changes slightly [6]. In contrast, in $Sr_{1-x}Bi_xMo_{1-x}V_xO_4$ doping with both Bi and V leads to the contraction of unit cell and by that means makes this oxide unstable. It can be assumed that such contraction decreases the distance between $[BO_4]^{n-}$ (B = Mo,V) clusters and, consequently, increases the repulsion between them. As a result, decomposition of $Sr_{1-x}Bi_xMo_{1-x}V_xO_4$ oxide is observed [20]. In general, Bi- and (Bi+V) doped $CaMoO_4$ and $SrMoO_4$ show the decreasing melting point temperature and, as a consequence, lower sintering temperature, as well as increasing conductivity, catalytic and photocatalytic activity. In addition, the shift of absorbance bands from UV to violet and blue parts of spectra was observed, and the energy gap decreases [6,22]. The last mentioned characteristics are important factors for such technical areas as photocatalytic oxidation under visible light or pigment technology.

Thus, the priority goal of the present work was to show the effects of bismuth and vanadium co-doping on the UV-VIS spectral characteristics and E_g values of the $Ca_{1-1.5x-y}Bi_{x+y}\Phi_xMo_{1-y}V_yO_4$ and $Sr_{1-1.5x-y}Bi_{x+y}\Phi_xMo_{1-y}V_yO_4$ complex oxides.

2. Experimental

Samples of $Ca_{1-1.5x-y}Bi_{x+y}\Phi_xMo_{1-y}V_yO_4$ and $Sr_{1-1.5x-y}Bi_{x+y}\Phi_xMo_{1-y}V_yO_4$ ($0 < x \leq 0.4$, $0 < y \leq 0.5$) were synthesised by conventional solid state methods from $SrCO_3$ (99.5%) or $CaCO_3$ (99.5%), Bi_2O_3 (99.9%), V_2O_5 (98.5%) and MoO_3 (99.0%) as starting materials. Stoichiometric amounts of dried precursors were weighed and mixed in an agate mortar as dispersions in ethanol. Mixed powders were then pelletized and calcined in steps at 550–720 °C with duration about 10 hours at each step followed by regrinding and re-pelletizing. The overall time of calcination was about 30 hours. X-ray powder diffraction (XRD) data were obtained using a Bruker Advance D8 diffractometer with a VANTEC1 detector (Ni filtered Cu Kα radiation, θ/θ geometry). XRD data were collected in the 2θ range of 6–120°, with steps of 0.02103° and an effective scan time of 200 s per step.

The reflection spectra were obtained in the range of 190–1100 nm by using a spectrophotometer Evolution 300 (Termo Sci) equipped with an integrating sphere. The absorption coefficient curves were derived from reflection curves using Kubelka-Munk model. Energy gaps for direct interband transitions were calculated with linear approximation of Kubelka-Munk function [21].

3. Results and Discussion

As-prepared samples of nominal composition $Ca_{1-1.5x-y}Bi_{x+y}\Phi_xMo_{1-y}V_yO_4$ and $Sr_{1-1.5x-y}Bi_{x+y}\Phi_xMo_{1-y}V_yO_4$ ($0 < x \leq 0.5$, $0 < y \leq 0.5$) were found to contain one phase for $y \leq 0.05$ ($x = 0$) and $y \leq 0.2$ ($x = 0$) for $CaMoO_4$- and $SrMoO_4$-based systems, respectively, although the solubility limit of vanadium in $Ca_{1-y}Bi_yMo_{1-y}V_yO_4$ is reported to be $y = 0.9$ [6,22]. $BiVO_4$ was also detected in $CaMoO_4$-based samples with $x = 0$ and $0.2 < y \leq 0.5$. Presence of $BiVO_4$ was also found in $Ca_{1-y}Bi_yMo_{1-y}V_yO_4$ ($0.4 < y \leq 0.9$) [22], but this fact was disregarded by authors during solid solution limits discussion. At low x concentration the sheelite structure are observed. But for oxides with higher x values the additional peaks in the XRD patterns are evident. These oxides were found to have the tetragonal supercell with $a_{sup} \approx \sqrt{5}a$, $c_{sup} \approx c$, where a and c are the tetragonal scheelite cell parameters, like it was found earlier for $Ca_{1-3x}Bi_{2x}Mo_1O_4$ [19] and $Sr_{1-3x}Bi_{2x}Mo_1O_4$ [20]. The areas of solid solutions (ordinary scheelite and superstructured scheelite) and inveatigated fields of triple phase diagram are shown at Fig. 1. It is seen that continuation of solid

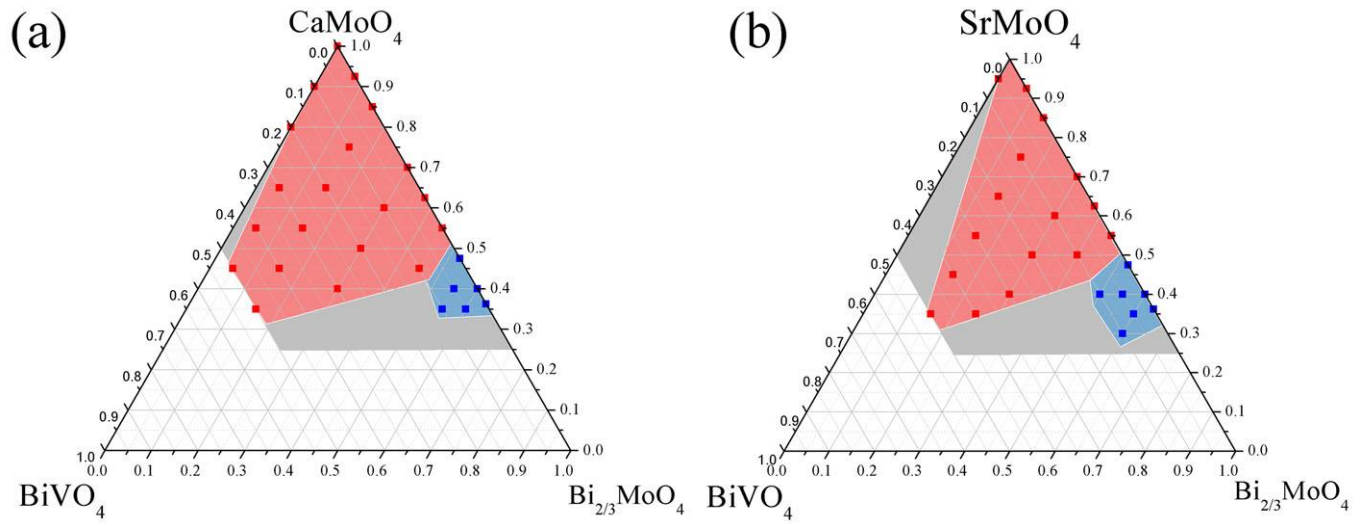

Fig. 1 The areas of scheelite-type solid solutions (red), superstructured scheelite solid solutions (blue) and tree-phases areas (gray) in $CaMoO_4$ - $BiVO_4$ - $Bi_2Mo_3O_{12}$ (a) and $SrMoO_4$ - $BiVO_4$ - $Bi_2Mo_3O_{12}$ (b) ternary diagram. White regions are unstudied areas ($x > 0.5$, $y > 0.5$).

solutions areas can be expected for $\{0.5 < x \leq 0.7, 0.5 < y \leq 0.6\}$ values. Compositions without solid solutions areas contain additional Bi_3MoO_{12} and monoclinic $BiVO_4$.

Previously, free refinement of the occupancies in superstructured $Ca_{1-3x}Bi_{2x}Mo_1O_4$ solid solutions showed the *4b* site positions to be fully occupied by bismuth, the *16f* site positions are partially occupied by both Ca^{2+} and Bi^{3+}[19]. In the present work, the refinement of the occupancies of *4b* and *16f* sites revealed the same pattern of doping.

It can be clearly observed that high concentration of bismuth only (i.e. $x+y$ values) does not lead to the superstructural ordering, but relatively high concentration of cationic vacancies accompanying high concentrations of bismuth provide the ordering of bismuth at *4b* position. Samples with superlattice ordering contain plains which include only bismuth and molybdenum atoms (Fig. 2) and the formation of such planes can be associated with preferred orientation of $6S^2$ lone pair electrons of bismuth along *z* axis. High concentration of cationic vacancies in *16f* Sr/Bi position provides required geometrical factors of favourable orientation of $6S^2$ lone pair and, as a result, the mentioned planes are formed.

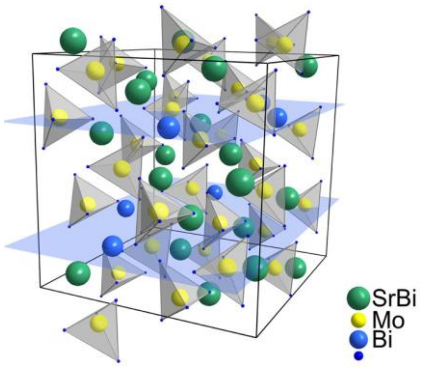

Fig. 2 Planes including Bi *4b* positions show the ordering of bismuth atoms in tetragonal supercell. "SrBi" *16f* positions are mixed with Sr, Bi and *Φ*.

The dependencies of the unit cell parameters for $Ca_{1-1.5x-y}Bi_{x+y}\Phi_xMo_{1-y}V_yO_4$ and $Sr_{1-1.5x-y}Bi_{x+y}\Phi_xMo_{1-y}V_yO_4$ compositions are shown in Fig. 3. The compression and enlargement are caused by substitution by smaller of bigger cation, respectively (ionic radii $r_{Ca^{2+}}$ = 1.12 Å, $r_{Sr^{2+}}$ = 1.26 Å, $r_{Bi^{3+}}$ = 1.17 Å [23]).

The ionic radius of vanadium is smaller than that of molybdenum ($r_{Mo^{6+}_{IV}}$ = 0.41 Å, $r_{V^{5+}_{IV}}$ = 0.355 Å), and V-doping impedes expansion of the unit cell in the case of $Ca_{1-1.5x-y}Bi_{x+y}\Phi_xMo_{1-y}V_yO_4$ and promotes the decrease of cell volume in the case of $Sr_{1-1.5x-y}Bi_{x+y}\Phi_xMo_{1-y}V_yO_4$. In both cases, the superstructural ordering is a "growth factor" of *c*-parameter. It leads to the sharp rise of *c*-parameter or local plateau on *c*-parameter dependence in the cases of $Ca_{1-1.5x-y}Bi_{x+y}\Phi_xMo_{1-y}V_yO_4$ and $Sr_{1-1.5x-y}Bi_{x+y}\Phi_xMo_{1-y}V_yO_4$, respectively. Probably, it is caused by stereochemical activity of $6S^2$ lone pair of bismuth in the planes parallel to *(xoy)* plane.

Typical diffuse scattering spectra of $(Ca/Sr)_{1-1.5x-y}Bi_{x+y}\Phi_xMo_{1-y}V_yO_4$ compositions are similar (Fig. 4). The scattering in the range of ~500–1100 nm is close to 100%. The spectra for $CaMoO_4$ and $SrMoO_4$ contain a broad band in the range of wavelengths ~200–300 nm that corresponds to electronic transition within the MoO_4^{2-} complex [24]. For Bi-doped and (Bi+V) -doped samples this band is located in higher wavelengths (see Fig. 4). The separate absorbance bands that correspond to transitions in the vanadium-oxygen complex are not observed. The band gap calculations for $(Ca/Sr)_{1-1.5x-y}Bi_{x+y}\Phi_xMo_{1-y}V_yO_4$ were carried out by using Kublenka-Munk theory and Tauc relation. Fig. 5 shows the Tauc plot for some compositions. The graph consists of non-linear and linear regions. The value of E_g can be obtained by drawing a tangent on the linear part. The point of inflection on the X-axis provides the value of band gap for the prepared powders.

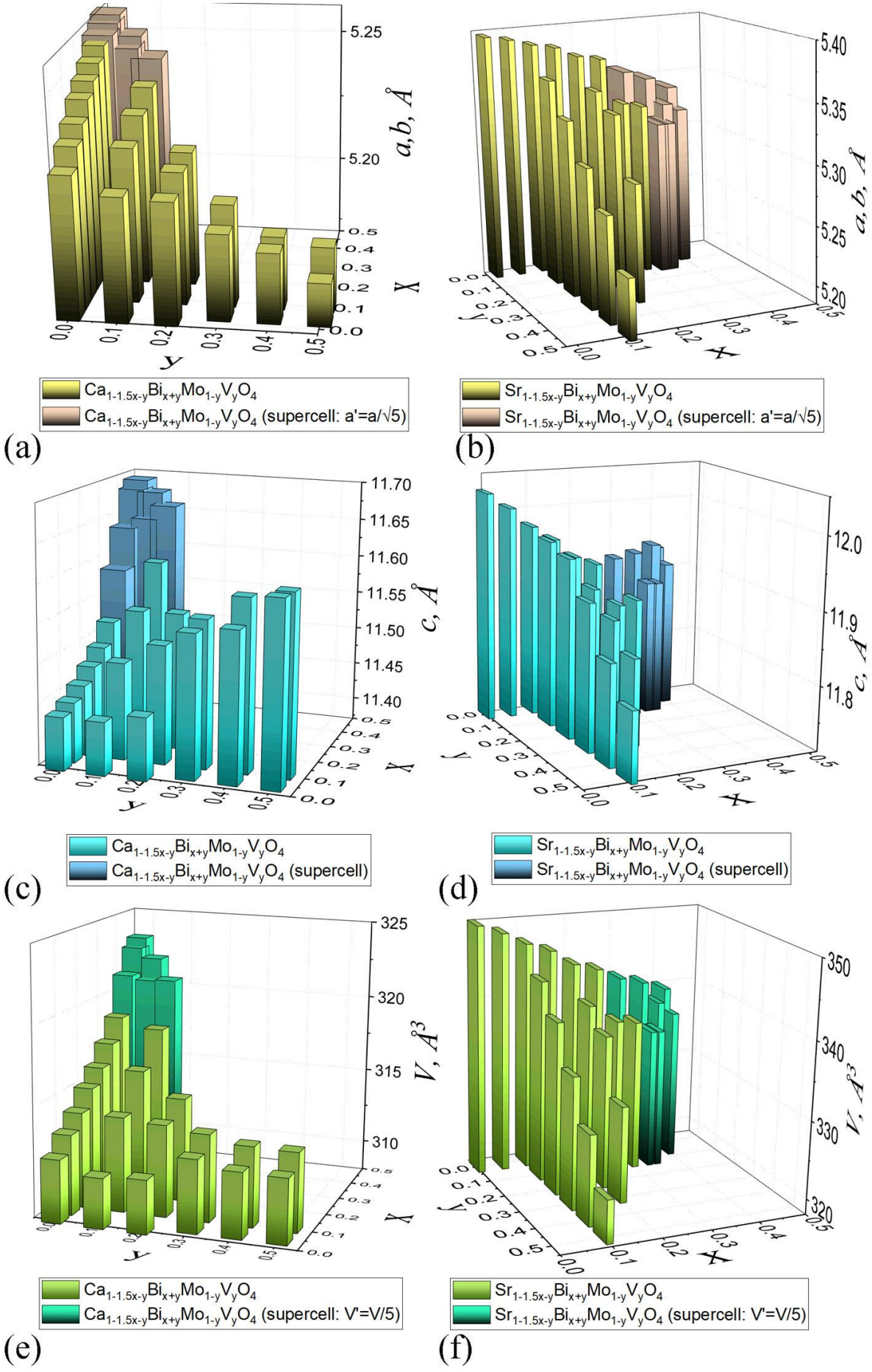

Fig. 3 The unit cell parameters depending on x and y parameters in $Ca_{1-1.5x-y}Bi_{x+y}\Phi_xMo_{1-y}V_yO_4$ (a,c,e) and $Sr_{1-1.5x-y}Bi_{x+y}\Phi_xMo_{1-y}V_yO_4$ (b,d,f) solid solutions

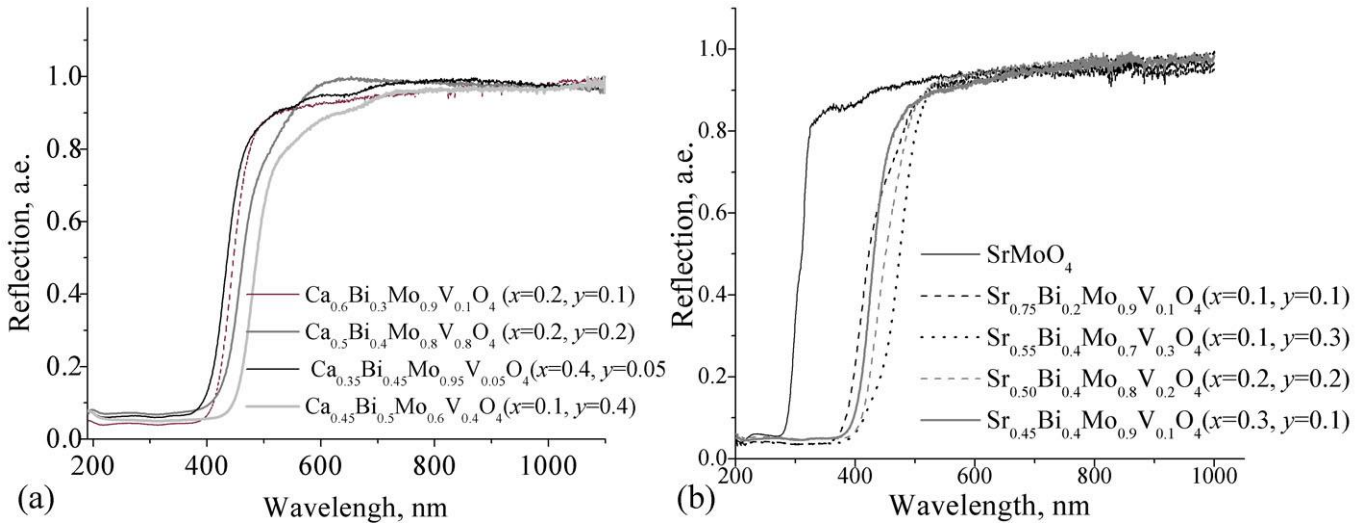

Fig. 4 The diffuse scattering spectra for some $Ca_{1-1.5x-y}Bi_{x+y}\Phi_xMo_{1-y}V_yO_4$ (a) and $Sr_{1-1.5x-y}Bi_{x+y}\Phi_xMo_{1-y}V_yO_4$ (b) compositions

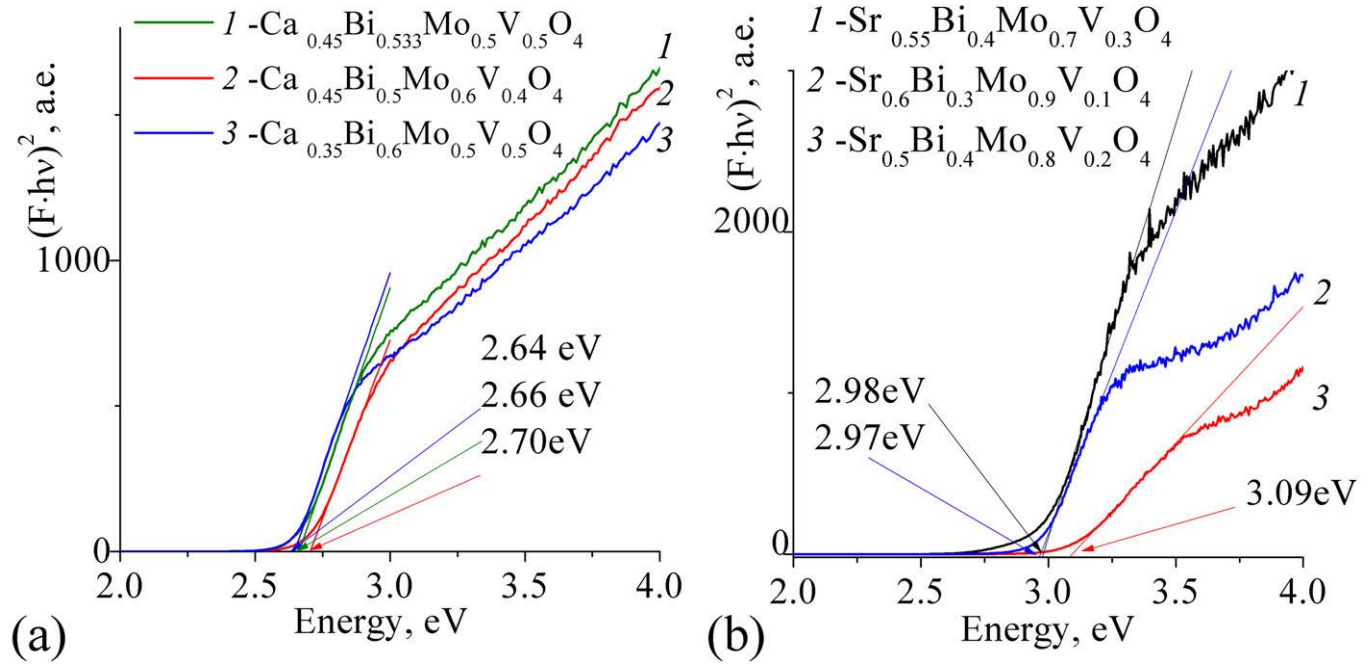

Fig. 5 Tauc plots for some $Ca_{1-1.5x-y}Bi_{x+y}\Phi_xMo_{1-y}V_yO_4$ (a) and $Sr_{1-1.5x-y}Bi_{x+y}\Phi_xMo_{1-y}V_yO_4$ (b) compositions

Calculated values of the band gap (E_g) for $Ca_{1-1.5x-y}Bi_{x+y}\Phi_xMo_{1-y}V_yO_4$ were found to be 3.83–2.64 eV for {x = 0, y = 0} – {x = 0.1, y = 0.5}compositions. E_g values for $Sr_{1-1.5x-y}Bi_{x+y}\Phi_xMo_{1-y}V_yO_4$ were 4.25–2.87 eV for {x = 0, y = 0} – {x = 0.2, y = 0.3} compositions. It is seen that the band gap value decreases with x and y (Fig. 6), and it reduces not only with bismuth content ($x+y$ value) but with vanadium content (y) as well. For $CaMoO_4$-based solid oxides, E_g value slowly decreases with x and rapidly decreases with y, while for $SrMoO_4$-based solid oxides we observed the opposite trends (Fig. 6). In general, the energy gap in $(Ca/Sr)_{1-1.5x-y}Bi_{x+y}\Phi_xMo_{1-y}V_yO_4$ is reduced by additional bands of Bi 6p electrons and by modification of states of Mo 4d electrons caused by distortion of MoO_4 polyhedra. Bands of Bi 6p electrons lead to the significant decrease of E_g even for low concentration of bismuth for both series of molybdates. In the case of distortion of MoO_4 polyhedra for $SrMoO_4$-based solid oxides, the sufficient contraction of the unit cell is observed, while for $CaMoO_4$-based solid oxides the cell volume grows. Therefore, the distortion of MoO_4 polyhedra caused by the formation of cation vacancies (represented by x while y = 0) is generally smaller for $CaMoO_4$-based compounds than that for $SrMoO_4$-based compounds. Strongly distorted MoO_4 polyhedra in $SrMoO_4$-based compounds do not change significantly at vanadium doping (y > 0), but weakly distorted MoO_4 polyhedra in $CaMoO_4$-based compounds show a sharp alteration at the same time. Meanwhile, some special effects for superstructured phases are not observed. For the purpose of E_g minimization, therefore, the best compositions are found to be {x = 0.1–0.2, y = 0.4–0.5} and {x = 0.2–0.425, y = 0.1–0.2} for $CaMoO_4$-

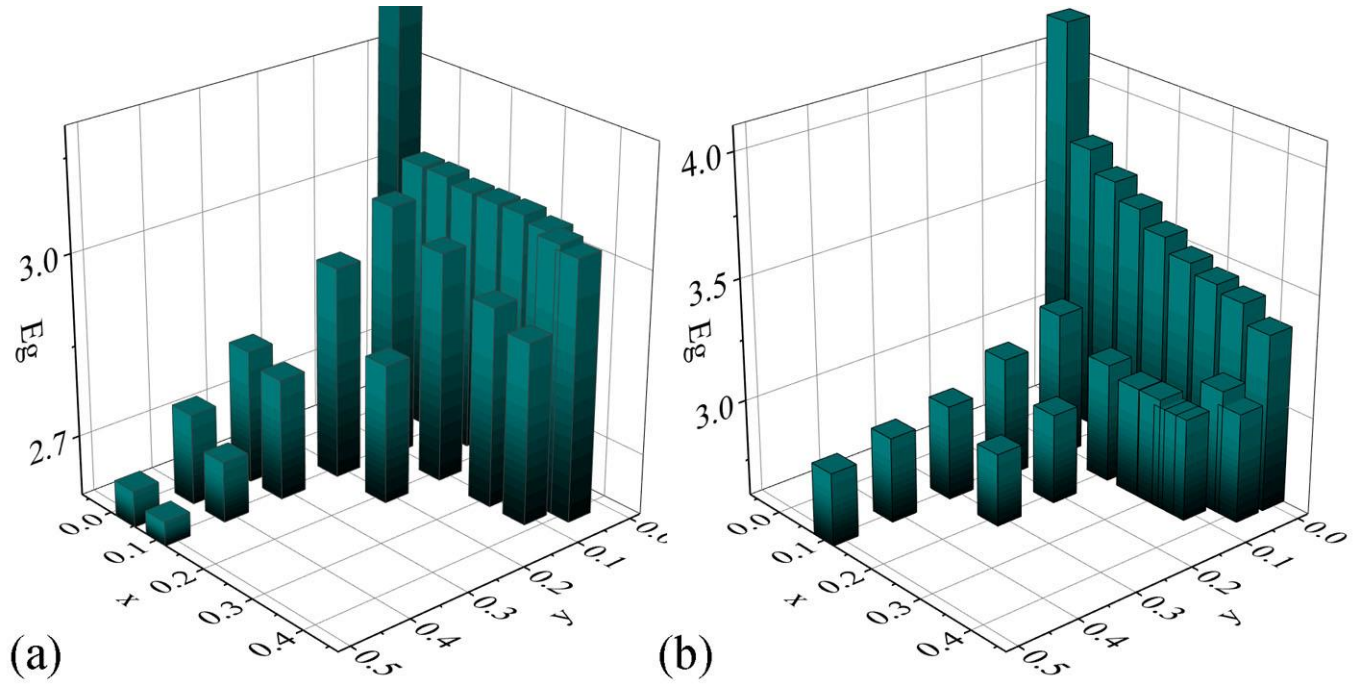

Fig. 6 The E_g changing in $Ca_{1-1.5x-y}Bi_{x+y}\Phi_xMo_{1-y}V_yO_4$ (a) and $Sr_{1-1.5x-y}Bi_{x+y}\Phi_xMo_{1-y}V_yO_4$ (b) series

based and $SrMoO_4$-based compounds, respectively. These compositions are expected to be the most effective photocatalysts in $(Ca/Sr)_{1-1.5x-y}$ $Bi_{x+y}\Phi_xMo_{1-y}V_yO_4$ series because of absorption of energy in both UV and vis (i.e. blue) parts of spectra.

4. Conclusions

Compounds with general formulae of $Ca_{1-1.5x-y}Bi_{x+y}\Phi_xMo_{1-y}V_yO_4$ and $Sr_{1-1.5x-y}Bi_{x+y}\Phi_xMo_{1-y}V_yO_4$ were synthesized by conventional solid state technique in the temperature range of 550–720 °C. The areas of solid solutions (ordinary scheelite and superstructured scheelite) were determined. It was observed that relatively high concentration of cationic vacancies accompanying high concentrations of bismuth provide the ordering of bismuth at *4b* position. The diffuse scatering spectra of homogeneous samples contain a broad band in the range of ~200–450 nm. Energy gaps, calculated with linear approximation of Kubelka-Munk function, decrease with bismuth content. The compositions with minimal E_g are found to be {x = 0.1–0.2, y = 0.4–0.5} and {x = 0.2–0.425, y = 0.1–0.2} for $CaMoO_4$-based and $SrMoO_4$-based compounds, respectively. These compositions are expected to be the most effective photocatalysts in $(Ca/Sr)_{1-1.5x-y}$ $Bi_{x+y}\Phi_xMo_{1-y}V_yO_4$ series.

Acknowledgements

The XPRD data were obtained in Ural-M center of Institute for Metallurgy, Ural Br. of RAS This work is supported by grant of RSF, project № 20-73-10048.

References

1. Frank M, Smetanin SN, Jelínek M, Vyhlídal D, Kopalkin AA, Shukshin VE, Ivleva LI, Zverev PG, Kubeček V. Synchronously-pumped all-solid-state $SrMoO_4$ Raman laser generating at combined vibrational Raman modes with 26-fold pulse shortening down to 1.4 ps at 1220 nm. Opt Laser Technol. 2019;111:129-33. doi:10.1016/j.optlastec.2018.09.045
2. Kunzel R, Umisedo NK, Okuno E, Yoshimura EM, Marques AP. Effects of microwave-assisted hydrothermal treatment and beta particles irradiation on the thermoluminescence and optically stimulated luminescence of $SrMoO_4$ powders. Ceram Int. 2020;46(10):15018-26. doi:10.1016/j.ceramint.2020.03.032
3. Yu H, Shi, X, Huang L, Kang X, Pan D. Solution-deposited and low temperature-annealed Eu^{3+}/Tb^{3+}-doped $CaMoO_4/SrMoO_4$ luminescent thin films. J Lumin. 2020;225:117371. doi:10.1016/j.jlumin.2020.117371
4. Elakkiya V, Sumathi S. Low-temperature synthesis of environment-friendly cool yellow pigment: Ce substituted $SrMoO_4$. Mater Lett. 2019;263:127246. doi:10.1016/j.matlet.2019.127246
5. Mikhailik VB, Elyashevskyi Yu, Kraus H, Kim HJ, Kapustianyk V, Panasyuk M. Temperature dependence of scintillation properties of $SrMoO_4$. Nucl Instrum Methods Phys Res A. 2015;792:1-5. doi:10.1016/j.nima.2015.04.018
6. Guo HH, Zhou D, Pang LX, Qi ZM. Microwave dielectric properties of low firing temperature stable scheelite structured $(Ca,Bi)(Mo,V)O_4$ solid solution ceramics for LTCC applications. J Eur Ceram Soc. 2019;39(7):2365-73. doi:10.1016/j.jeurceramsoc.2019.02.010
7. Yu-Ling Y, Xue-Ming L, Wen-Lin F, Wu-Lin L, Chuan-Yi T. Co-precipitation synthesis and photoluminescence properties of $(Ca_{1-x-y}Ln_y)MoO_4$: xEu^{3+} (Ln =Y, Gd) red phosphors. J Alloys Compd. 2010;505(1):239-42. doi:10.1016/j.jallcom.2010.06.037
8. Zhu Y, Zheng G, Dai Z, Zhang L, Ma Y. Photocatalytic and luminescent properties of $SrMoO_4$ phosphors prepared via hydrothermal method with different stirring speeds. J Mater Sci Technol. 2017;33(1):23-39. doi:10.1016/j.jmst.2016.11.019
9. Yao Z-F, Zheng G-H, Dai Z-X, Zhang L-Y. Synthesis of the Dy: $SrMoO_4$ with high photocatalytic activity under visible light irradiation. Appl Organomet Chem. 2018;32(8):e4412. doi:10.1002/aoc.4412

10. Wang Y, Xu H, Shao C, Cao J. Doping induced grain size reduction and photocatalytic performance enhancement of $SrMoO_4$:Bi^{3+}. Appl Surf Sci. 2017;392:649-57. doi:10.1016/j.apsusc.2016.09.09
11. Vidya S, John A, Solomon S, Thomas J. Optical and dielectric properties of $SrMoO_4$ powders prepared by the combustion synthesis method. Adv Mater Res. 2012;1:191-204. doi:10.12989/amr.2012.1.3.191
12. Cheng J, Liu C, Cao W, Qi M, Shao G. Synthesis and electrical properties of scheelite $Ca_{1-x}Sm_xMoO_{4+d}$ solid electrolyte ceramics. Mater Res Bull. 2011;46(2):185-9. doi:10.1016/j.materresbull.2010.11.019
13. Guo J, Randall CA, Zhou D, Zhang G, Zhang C, Jin B, Wang H. Correlation between vibrational modes and dielectric properties in $(Ca_{1-3x}Bi_{2x}\square_x)MoO_4$ ceramics. J Eur Ceram Soc. 2015;35(3):4459-64. doi:10.1016/j.jeurceramsoc.2015.08.020
14. Pang L-X, Sun G-B, Zhou D. $Ln_2Mo_3O_{12}$ (Ln = La, Nd): A novel group of low loss microwave dielectric ceramics with low sintering temperature. Mater Lett. 2011;65(2):164-6. doi:10.1016/j.matlet.2010.09.064
15. Esaka T. Ionic conduction in substituted scheelite-type oxides. Solid State Ionics. 2000;136-137(1-2):1-9. doi:10.1016/s0167-2738(00)00377-5
16. Yang X, Wang Y, Wang N, Wang S, Gao G. Effects of co-doped Li^+ ions on luminescence of CaWO4:Sm^{3+} nanoparticles. J Mater Sci Mater Electronics. 2014;25:3996-4000. doi:10.1007/s10854-014-2119-4
17. Jiang P, Gao W, Cong R, Yang T. Structural investigation of the A-site vacancy in scheelites and the luminescence behavior of two continuous solid solutions $A_{1-1.5x}Eu_x\square_{0.5x}WO_4$ and $A_{0.64-0.5y}Eu_{0.24}Li_y\square_{0.12-0.5y}WO_4$ (A = Ca, Sr; $\square$ = vacancy). Dalton Trans. 2015;44(13):6175-83. doi:10.1039/c5dt00022j
18. Sleight JAW, Aykan K. New nonstoichiometric molybdate, tungstate, and vanadate catalysts with the scheelite-type structure. J Solid State Chem. 1975;13(4):231-6. doi:10.1016/0022-4596(75)90124-3
19. Mikhaylovskaya ZA, Abrahams I, Petrova SA, Buyanova ES, Tarakina NV, Piankova DV, Morozova MV. Structural, photocatalytic and electroconductive properties of bismuth-substituted $CaMoO_4$. J Solid State Chem. 2020;291:121627. doi:10.1016/j.jssc.2020.121627
20. Mikhaylovskaya ZA, Buyanova ES, Petrova SA, Nikitina AA. Sheelite-related strontium molybdates: synthesis and characterization. Chimica Techno Acta 2018;5(4):189-95. doi:10.15826/chimtech.2018.5.4.03
21. Kay MI, Frazer BC, Almodovar I. Neutron diffraction refinement of $CaWO_4$. J Chem Phys. 1964;40(2):504-506. doi:10.1063/1.1725144
22. Yao W, Ye J. Photophysical and photocatalytic properties of $Ca_{1-x}Bi_xV_xMo_{1-x}O_4$ solid solutions. J Phys Chem B. 2006;110:11188-95. doi:10.1021/jp0608729
23. Shannon RD. Revised effective ionic radii and systematic studies of interatomic distances in halides and chalcogenides. Acta Cryst. 1976;A32:751–67. doi:10.1107/S0567739476001551
24. Verma A, Sharma SK. Rare-earth doped/codoped $CaMoO_4$ phosphors: A candidate for solar spectrum conversion. Solid State Sci. 2019;96:105945. doi:10.1016/j.solidstatesciences.2019.105945